# Mitochondria Permeability Transition versus Necroptosis in Oxalate-Induced AKI

Shrikant Ramesh Mulay [iD],[1,2] Mohsen M. Honarpisheh,[1] Orestes Foresto-Neto [iD],[1]
Chongxu Shi,[1] Jyaysi Desai,[1] Zhi Bo Zhao,[1] Julian A. Marschner,[1] Bastian Popper,[3]
Ewa Miriam Buhl,[4] Peter Boor,[4] Andreas Linkermann,[5] Helen Liapis,[6,7] Rostyslav Bilyy,[8]
Martin Herrmann,[9] Paola Romagnani,[10] Ilya Belevich [iD],[11] Eija Jokitalo [iD],[11] Jan U. Becker,[12]
and Hans-Joachim Anders [iD] [1]

Due to the number of contributing authors, the affiliations are listed at the end of this article.

## ABSTRACT

**Background** Serum oxalate levels suddenly increase with certain dietary exposures or ethylene glycol poisoning and are a well known cause of AKI. Established contributors to oxalate crystal–induced renal necroinflammation include the NACHT, LRR and PYD domains-containing protein-3 (NLRP3) inflammasome and mixed lineage kinase domain-like (MLKL) protein–dependent tubule necroptosis. These studies examined the role of a novel form of necrosis triggered by altered mitochondrial function.

**Methods** To better understand the molecular pathophysiology of oxalate-induced AIK, we conducted *in vitro* studies in mouse and human kidney cells and *in vivo* studies in mice, including wild-type mice and knockout mice deficient in peptidylprolyl isomerase F (Ppif) or deficient in both Ppif and Mlkl.

**Results** Crystals of calcium oxalate, monosodium urate, or calcium pyrophosphate dihydrate, as well as silica microparticles, triggered cell necrosis involving PPIF–dependent mitochondrial permeability transition. This process involves crystal phagocytosis, lysosomal cathepsin leakage, and increased release of reactive oxygen species. Mice with acute oxalosis displayed calcium oxalate crystals inside distal tubular epithelial cells associated with mitochondrial changes characteristic of mitochondrial permeability transition. Mice lacking Ppif or Mlkl or given an inhibitor of mitochondrial permeability transition displayed attenuated oxalate-induced AKI. Dual genetic deletion of *Ppif* and *Mlkl* or pharmaceutical inhibition of necroptosis was partially redundant, implying interlinked roles of these two pathways of regulated necrosis in acute oxalosis. Similarly, inhibition of mitochondrial permeability transition suppressed crystal-induced cell death in primary human tubular epithelial cells. PPIF and phosphorylated MLKL localized to injured tubules in diagnostic human kidney biopsies of oxalosis-related AKI.

**Conclusions** Mitochondrial permeability transition–related regulated necrosis and necroptosis both contribute to oxalate-induced AKI, identifying PPIF as a potential molecular target for renoprotective intervention.

Crystal nephropathies are forms of AKI or CKD induced by solid particles of various sizes and shapes composed of atoms, ions, or biomolecules.[1,2] Crystal nephropathies can be categorized in three types depending from the localization of the crystals inside afferent blood vessels (type 1), inside the nephron (type 2), or inside the renal pelvis and ureter (type 3).[1] Acute oxalosis is a paradigmatic form of a type 2 crystal–induced AKI that occurs upon incident exposures to oxalate-rich food or drinks, vitamin C supplements, and during

ethylene glycol poisoning.[3–5] Increased intestinal adsorbtion of oxalate, *e.g.*, after bypass surgeries, can contribute to secondary hyperoxaluria.[6] In acute oxalosis, calcium oxalate monohydrate and bihydrate (CaOx) crystals form in the distal tubule. They grow to crystal plugs that obstruct the tubular lumen in some nephrons but are also widely taken up into tubular epithelial cells and even reach the interstitial space.[1] We recently described that CaOx crystals trigger renal inflammation *via* the NLRP3 inflammasome- and caspase-1–mediated secretion of IL-1$\beta$ in intrarenal dendritic cells,[7] a process largely contributing to AKI. We subsequently described that crystals also exert a direct cytotoxic effect on tubular cells in acute oxalosis by inducing necroptosis, a receptor-interacting serine-threonine kinase-3 (RIPK3)–dependent and mixed lineage kinase domain-like (MLKL)–dependent form of regulated tubular cell necrosis.[8] However, genetic deletion or pharmaceutic inhibition of necroptosis only partially abrogated cytotoxicity of CaOx crystals. We hypothesized that another of the recently identified forms of regulated cell death[9] could be involved in CaOx crystal–induced AKI and speculated on mitochondrial permeability transition (MPT)–related cell necrosis,[9,10] because a suitable inhibitor was previously shown to limit renal cell death in a rat model of oxalate nephropathy.[11] This pathway is characterized by mitochondrial dysfunction involving a peptidylprolyl isomerase F (PPIF; also named cyclophilin D/F)-driven formation and permanent opening of the MPT pore, disruption of the mitochondrial outer membrane potential, mitochondrial swelling, loss of cristae, and potentially the release of reactive oxygen species (ROS) into the cytosol.[9,10,12] Indeed, our studies propose MPT in concert with necroptosis promote cytotoxicity of CaOx and numerous other crystals, implying MPT/necroptosis as molecular targets to limit CaOx crystal–induced AKI.

## METHODS

### Cell Culture Studies

Murine L929 cells were maintained in DMEM/F12 (GIBCO, Invitrogen, Carlsbad, CA) containing 10% FCS and 1% penicillin-streptomycin. Primary tubular epithelial cells were isolated from kidneys of *Ppifd*$^{+/+}$ and *Ppifd*$^{-/-}$ mice (original strain Ppif$^{tm1Jmol}$/J, Jackson Laboratories stock no. 009071) and were maintained in DMEM/F12 containing 10% FCS, 1% penicillin-streptomycin, 125 ng/ml PG E1 (Calbiochem, Darmstadt, Germany), 25 ng/ml EGF, 1.8 $\mu$g/ml l-thyroxine, 3.38 ng/ml hydrocortisone, and 2.5 mg/ml of insulin-transferrin-sodium selenite supplement (all from Sigma-Aldrich, Munich, Germany unless mentioned). Human renal progenitor cells were prepared from human kidney tissues using standard sieving technique through graded mesh screens (60, 80, 150, and 200 mesh).[13] Cells were grown to confluence before use in experiments. Human kidney cells (HK-2) were maintained in RPMI (GIBCO, Invitrogen) containing 10%

### Significance Statement

Sudden increases in serum oxalate levels occurring with certain dietary exposures or ethylene glycol poisoning are a well known cause of AKI. The authors recently reported that intrarenal precipitation of calcium oxalate crystals activates NACHT, LRR, and PYD domains-containing protein-3 (NLRP3)–dependent inflammation and mixed lineage kinase domain-like (MLKL) protein-dependent tubule necroptosis, *i.e.*, renal necroinflammation. In this study, they show that calcium oxalate crystals and other microparticles activate another route of regulated cell necrosis, peptidylprolyl isomerase F (PPIF)–dependent mitochondrial permeability transition, a process involving crystal phagocytosis and lysosomal destabilization. Mice deficient in Ppif or treated with an inhibitor of mitochondrial permeability transition were protected from oxalate-induced AKI. These results point to a previously unknown pathomechanism of type 2 crystal nephropathies and identify a potential molecular target for renoprotective intervention.

FCS and 1% penicillin-streptomycin. The cell lines, originally from American Type Culture Collection, were kindly provided by Peter Nelson (HK-2) and Bruno Luckow (L929), both from Ludwig Maximilian University (Munich, Germany). All cell lines used were tested for mycoplasma contamination before use. All cells were stimulated with crystals of CaOx (1000 $\mu$g/ml, 1–2 $\mu$m size) (Alfa aesar, Karlsruhe, Germany), silica (500 $\mu$g/ml, 1–5 $\mu$M size) (Alfa aesar), monosodium urate (MSU; 1000 $\mu$g/ml, 25–125 nm size) (Invivogen, Toulouse, France), and calcium pyrophosphate dihydrate (CPPD; 500 $\mu$g/ml, 25–125 nm size) (Invivogen) in different experiments. Whenever required, 30 minutes before crystal stimulations cells were pretreated with the MPT inhibitor cyclosporine A (Sigma-Aldrich (0.5 and 1 $\mu$m), mitochondrial ROS inhibitor (2R, 4R)-4-aminopyrrolidine-2,4-dicarboxylate (APDC; Sigma-Aldrich) (100 and 200 $\mu$M), phagocytosis (actin-polymerization) inhibitor cytochalasin D (Calbiochem) (5 and 10 $\mu$M), and cathepsin inhibitor CA074Me (Calbiochem) (10 and 20 $\mu$M). All the cells were cultured in an incubator at 37°C, 5% $CO_2$. Mitochondrial outer membrane potential and ROS production were measured using tetramethylrhodamine ethyl ester (TMRE; Invitrogen), lysotracker (Abcam, Cambridge, UK), and dichlorofluorescin diacetate (DCFDA) dyes (Sigma-Aldrich), respectively, according to the manufacturer's protocol. Calcein (Invitrogen) was used to identify live cells, whereas propidium iodide (Invitrogen) was used to identify dead cells according to the manufacturer's protocol. Fluorescence signals were detected using Leica fluorescence microscope (Leica, Wetzlar, Germany), and quantified using ImageJ software. In addition, cell death was also evaluated using lactate dehydrogenase cell cytotoxicity assay kit (Roche, Mannheim, Germany) according to manufacturer's protocol.

### Serial Block Face Scanning Electron Microscopy Data Collection and Reconstruction

Kidney cells were fixed as above but stained using an enhanced staining protocol.[14] Stained and dehydrated specimens were embedded into Durcupan ACM resin (Merck, Sigma-Aldrich)

that was mixed according to the manufacturer's recommendations. The embedded tissue was trimmed to a pyramid and mounted onto a pin using conductive epoxy glue (model 2400; CircuitWorks, Kennesaw, GA). Finally, the sides of the pyramid were covered with silver paint (Agar Scientific Ltd., Stansted, UK), and the whole assembly was platinum coated using Quorum Q150TS (Quorum Technologies, Laughton, UK). Serial block face-scanning electron microscopy (SB-EM) datasets were acquired with an FEG-SEM Quanta 250 (Thermo Fisher Scientific, FEI, Hillsboro, OR), using a backscattered electron detector (Gatan Inc., Pleasanton, CA) with 2.5-kV beam voltage, a spot size of 3, and a pressure of 0.2 Torr. The block faces were cut with 30-nm increments and imaged with XY resolution of 22 nm per pixel. The collected 16-bit images were processed for segmentation using an open-source software Microscopy Image Browser[15] as follows: (1) individual images were combined into three-dimensional (3D) stacks, (2) the combined 3D stack was aligned, (3) the contrast for the whole stack was normalized, and (4) the images were converted to the eight-bit format. The collected dataset was cropped to include only cells containing crystals. The cropped dataset was filtered using BM3D filter[16] and segmented using the semiautomatic graphcut segmentation of MIB. The graphcut segmentation starts with clustering of voxels into 3D supervoxels using the watershed[17] (nucleus) or SLIC[18] (crystals and cell body) algorithms. An adjacency map of supervoxels with energy barriers required to travel from one supervoxel to another is calculated and these values are used to generate a mathematical graph. Using the provided seeds for background and each aforementioned organelles, the algorithm performs maxflow/mincut split of the graph[19] to generate the model. The final visualization of the model was done in Amira (Thermo Fisher Scientific).

### Animal Studies

$Ppifd^{-/-}$ mice were purchased from The Jackson Laboratories (stock no. 009071) and backcrossed to the C57BL/6J mice background. J. Murphy and W. Alexander (WEHI, Australia) kindly provided $Mlkl^{-/-}$ mice.[20] Wild-type mice were purchased from Charles River. All mice were housed in groups of five under specific pathogen-free and 12-hour light/dark cycle conditions with *ad libitum* access to food and water. To induce acute oxalate nephropathy, 6- to 8-week-old male mice received a single intraperitoneal injection of 100 mg/kg of sodium oxalate (Santa Cruz Biotechnology, Heidelberg, Germany) and 3% sodium oxalate in drinking water and kidneys were harvested after 24 hours (n=5–9 per group).[7,8] As a therapeutic strategy, mice received a single dose of either cyclosporine A (2 mg/kg, administered intravenously; Sigma-Aldrich) or necrostatin-1s (1.65 mg/kg, administered intraperitoneally; Millipore, Darmstadt, Germany) or combination before sodium oxalate injections (n=5–9 per group). Mice were euthanized by cervical dislocation after collecting blood and urine. One part of the kidneys was stored in RNA later solution at −20°C for RNA isolation. Another part of the kidney was stored in formalin to be embedded in paraffin for histologic analysis. Samples for electron microscopy were fixed in 4% glutaraldehyde. Mice were assigned different groups with the use of stratified randomization method. The local institutional animal ethics committee and government authorities (Regierung der Oberbayern) approved all experimental procedures. Humane end points, as in the ethical approval for the study, were monitored throughout the study. All animal studies were conducted according to the European equivalent of the National Institutes of Health's *Guide for the Care and Use of Laboratory Animals.*

### Human Samples

A retrospective search for CaOx deposits in a database of 92,000 medical and transplant renal biopsy specimens (Arkana Laboratories, Little Rock, AR) was performed (institutional review board approval number 05–4397–0). Paraffin sections were randomly selected from native kidney biopsy specimens with adequate residual tissue containing CaOx crystals (n=20), and stained with 1:500 rabbit anti pMLKL (#EPR9514; Abcam) and 1:100 rabbit anti CypD (LLC #NBP2–15079; Novus Biologicals, Littleton, CO) as per manufacturer's instructions. Antigens were retrieved using citrate buffer pH 6.0. Bound primary antibody was visualized with a standard horseradish peroxidase detection system in brown.

### Statistical Analyses

Data are presented as mean±SEM. A comparison of groups was performed using paired $t$ test, and one-way ANOVA with *post hoc* Bonferroni correction was used for multiple comparisons. A value of $P<0.05$ was considered to indicate statistical significance. We used GraphPad prism 5 software for statistical analysis. Further detailed descriptions on the experimental methods are provided in the supplemental appendix 1.

## RESULTS

### CaOx Crystal Cytotoxicity Involves MPT

First, we evaluated mitochondrial structure and function upon exposure to CaOx crystals and silica, *in vitro*. Both induced mitochondrial swelling, loss of cristae, loss of mitochondrial outer membrane potential, and release of ROS with subsequent cell necrosis (Figure 1, A–D). The cyclophilin (and hence MPT) inhibitor cyclosporin A fully reversed the membrane potential, whereas ROS inhibition with APDC did not (Figure 1E), indicating that ROS release is downstream of losing the mitochondrial membrane potential. In support of this finding, cyclosporin A and APDC both abrogated crystal-induced ROS production and cell necrosis (Figure 1, F and G). Similar results were obtained upon PPIF suppression with specific siRNA (Supplemental Figure 1, A and B) in L929 cells, as well as in primary tubular epithelial cells isolated from wild-type and *Ppif*-deficient mice (Supplemental Figure 1, C and D). Similar results were obtained for crystals of MSU and CPPD (Supplemental Figures 1–3), implying that these effects relate
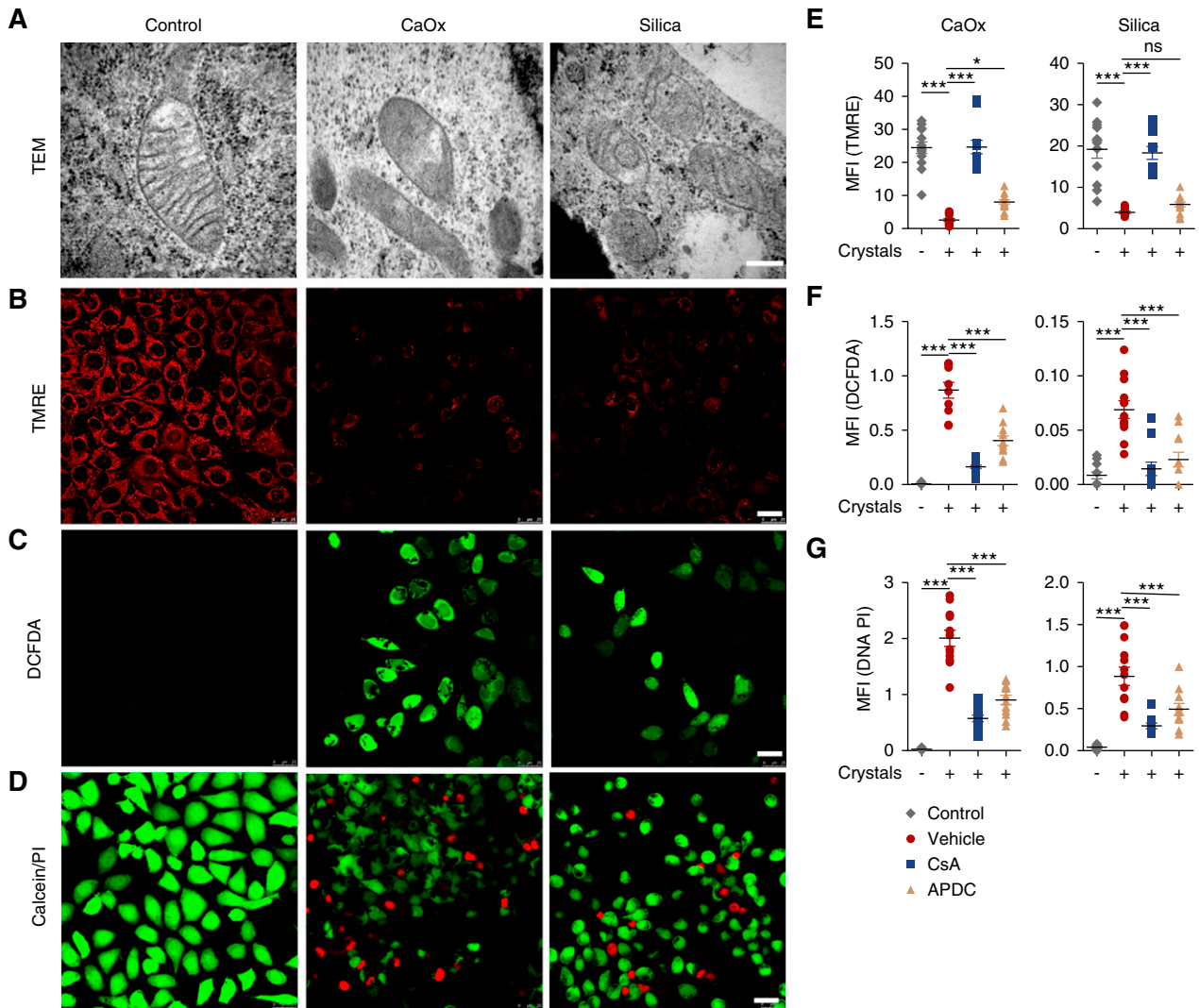
**Figure 1.** Crystal exposure leads to Ppif-dependent mitochondrial damage, subsequent ROS generation, and cell necrosis. (A–D) Crystals of CaOx and silica were incubated with L929 cells for 24 hours as indicated. (A) TEM images show that these crystals induce mitochondrial damage as indicated by loss of cristae and presence of swollen mitochondria (scale bar 250 nm). (B) Mitochondrial outer membrane potential (MOMP) was measured using TMRE dye. Images show loss of membrane potential upon exposure to crystals (scale bar 25 $\mu$m). (C) ROS was quantified using 2′,7′-dichlorodihydrofluorescein diacetate (DCFDA) dye. Images show the exposure of crystals leads to the generation of ROS (scale bar 25 $\mu$m). (D) Cell necrosis was measured using calcein for live cells (green) and PI for dead cells (red). Images indicate cellular necrosis upon crystal exposure (scale bar 25 $\mu$m). (E–G) Cells were pretreated with cyclosporine A (CsA) (1 $\mu$M) and antioxidant ammonium pyrrolidine dithiocarbamate (APDC; 200 $\mu$M) before exposing to crystals. After 24 hours, (E) MOMP and (F) ROS were quantified using TMRE and DCFDA positivity, respectively. (G) Cell necrosis was quantified using propidium iodide positivity. Results were expressed as mean fluorescence intensity (MFI) on digital analysis of pictures taken from culture dishes ($n$=10–12). Data are representative of three independent experiments. Data were analyzed using one-way ANOVA and are presented as mean±SEM. *$P<0.05$; ***$P<0.001$. n.s, not significant versus vehicle.

to particle structure rather than to the molecular type of crystal. Thus, crystal-related cell necrosis involves MPT with PPIF-driven loss of the mitochondrial outer membrane potential and ROS release as up- and downstream events, respectively.

### Crystal-Induced MPT Involves Crystal Phagocytosis and Lysosomal Leakage of Cathepsins

CaOx crystal phagocytosis, lysosomal destabilization, and leakage of lysosomal proteases such as cathepsins are involved in CaOx crystal–induced activation of the NLRP3 inflammasome and other cytosolic signaling pathways.[7,21,22] Indeed, two-dimensional (2D) transmission electron microscopy (TEM) and 3D SB-EM imaging studies documented phagocytosis of large amounts of CaOx crystals into endosomal compartments (Figure 2, A–C, Supplemental Videos 1 and 2). The 2D confocal microscopy documented crystal uptake into lysosomes and loss of TMRE positivity as a marker of an intact mitochondrial outer membrane potential (Figure 2, D and E).
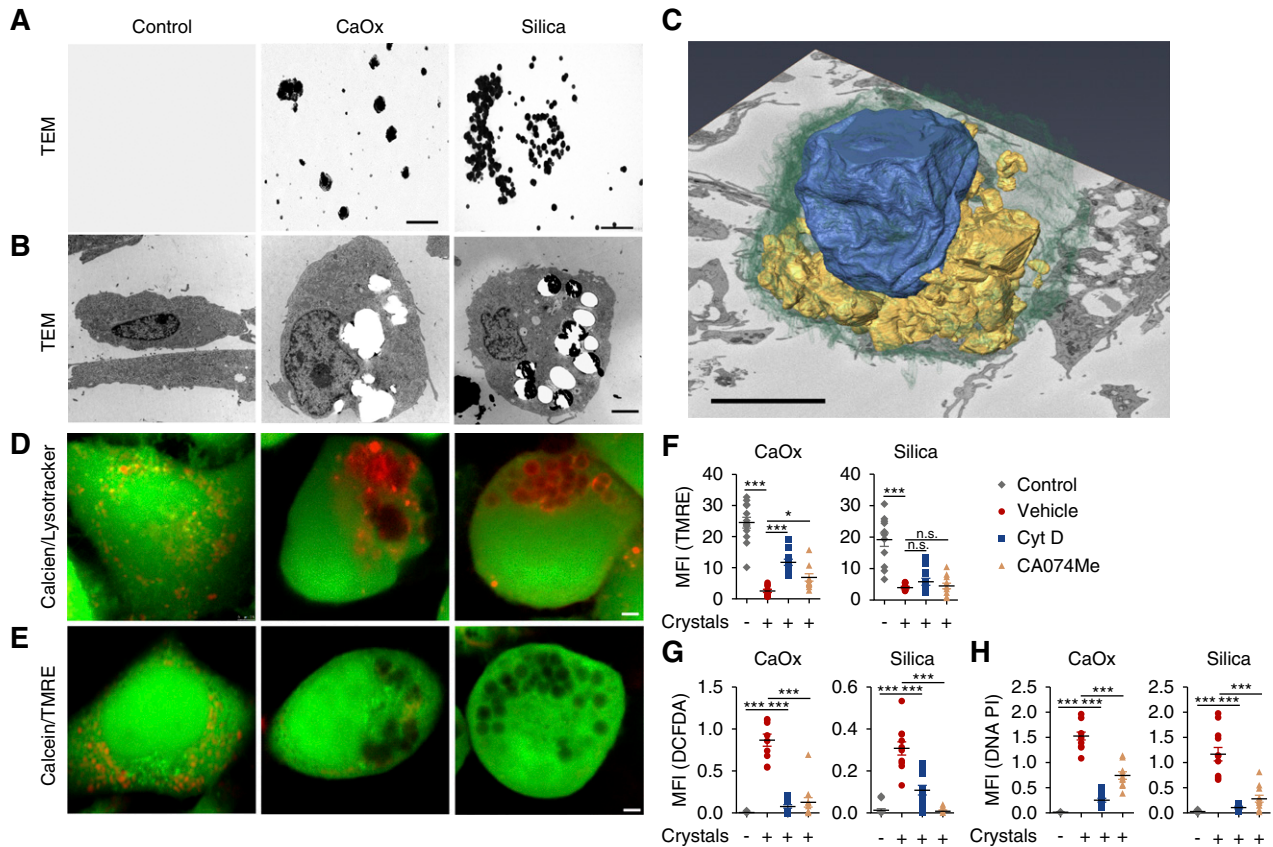
**Figure 2.** Phagocytosis of crystals and subsequent lysosome rupture precedes crystal-induced mitochondrial damage and cell necrosis. (A) 2D TEM images show different sizes and shapes of crystals of CaOx (scale bar 250 nm) and silica (scale bar 2 $\mu$m). (B–D) Crystals of CaOx and silica were incubated with L929 cells for 24 hours as indicated. (B) TEM images indicate crystal phagocytosis. Note that the crystals present within cells were washed out during processing, leaving behind voids in the cytosol. Some silica crystals can still be seen. (C) A 3D reconstruction from SB-EM images shows crystals phagocytosis (yellow) placed into a context of a cell (green) and its nucleus (blue); scale bar 5 $\mu$m. (D and E) Calcein staining reveals black spots inside cells, suggesting crystal phagocytosis. (D) Cells were costained with lysotracker to visualize lysosomes (red). Images show colocalization of lysosomes (red) and phagosomes (black spots in green), indicating phagolysosomes. (E) Cells were costained with TMRE (red) to access mitochondrial outer membrane potential (MOMP). Images show that exposure of crystals results in loss of MOMP, indicating mitochondrial damage. (F–H) Cells were pretreated with the phagocytosis inhibitor cytochalasin D (CytD) (10 $\mu$M) and the cathepsin inhibitor CA074Me (20 $\mu$M) before exposing to crystals. After 24 hours, (F) MOMP and (G) ROS were quantified using TMRE and 2′,7′-dichlorodihydrofluorescein diacetate (DCFDA) positivity, respectively. (H) Cell necrosis was quantified using propidium iodide positivity. Results were expressed as mean fluorescence intensity (MFI) on digital analysis of pictures taken from culture dishes ($n$=10–12). Data are representative of three independent experiments. Data were analyzed using one-way ANOVA and are presented as mean±SEM. *$P$<0.05; ***$P$<0.001. n.s, not significant versus vehicle.

Consistently, cytochalasin D, a phagocytosis inhibitor, partially prevented the CaOx crystal–induced loss of the TMRE signal and substantially suppressed ROS production and cell necrosis (Figure 2, F–H). Furthermore, the cathepsin inhibitor CA074Me prevented CaOx crystal–induced loss of mitochondrial outer membrane potential, ROS production, and cell necrosis (Figure 2, F–H). Similar data were obtained for MSU and CPPD crystals (Supplemental Figures 4 and 5). Therefore, we conclude that CaOx crystal uptake *via* phagocytosis into intracellular lysosomes promotes lysosomal cathepsin leakage as upstream events in crystal-induced MPT-regulated necrosis.

### *Ppif* Deficiency Attenuates CaOx Crystal–Induced AKI

To mimic hyperoxaluria-related AKI, we exposed mice to intraperitoneal sodium oxalate inducing intrarenal CaOx crystal deposition and AKI.[7,8,23] CaOx crystal plugs formed within proximal and distal tubules as evident from Pizzolato and hematoxylin and eosin stains, as well as *ex vivo* kidney microcomputed tomography (Figure 3, A–C, Supplemental Figure 6, A and B, Supplemental Video 3) and induced TUNEL+ cytotoxicity in proximal and distal tubules and sporadically also in collecting ducts (Supplemental Figure 7). The 3D reconstruction of SB-EM sections revealed large luminal crystal plugs and smaller crystals also within epithelial cells of the thick ascending limb of

the outer medulla (Figure 3D). In contrast to unaffected tubular segments, crystal-exposed epithelial cells exhibited mitochondrial ballooning (Figure 3, E and F). High-resolution TEM of such cells revealed loss of inner membrane cristae beyond ballooning as ultrastructural signs of MPT, water influx, and mitochondrial dysfunction (Figure 3, G–I). Indeed, advanced mitochondrial abnormalities were often seen in cells undergoing disintegration and detachment from the tubular basement membrane (Supplemental Figure 6C), *i.e.*, acute tubular necrosis. To test whether *Ppif* and MPT contributes to crystalline AKI, we induced oxalate nephropathy in wild-type and *Ppif*-deficient mice, which resulted in identical CaOx crystal deposits in both mouse strains (Figure 4A). Functional parameters of crystalline AKI (*i.e.*, plasma creatinine levels) and structural parameters of kidney injury (*i.e.*, tubular necrosis and TUNEL-positive cells) were significantly attenuated in *Ppif*-deficient mice (Figure 4, B–E). Thus, CaOx crystal–induced cell necrosis involves Ppif-driven MPT-RN also *in vivo*.

### MPT-RN and Necroptosis Both Contribute to CaOx Crystal Cytotoxicity *In Vivo*

To test for redundancy versus synergy between crystal-induced MPT-RN and necroptosis in oxalate crystal-induced AKI, we induced disease in mice with single versus dual genetic deletion of *Ppif* and *Mlkl*. Oxalate exposure induced equal amounts of CaOx crystal deposits in all mouse strains (Figure 4A). Lack of Mlkl showed a similar protection from AKI and tubular injury as compared with lack of Ppif (Figure 4, B–E). Dual gene deficiency for *Ppif* and *Mlkl* revealed a significant additive effect on tubular injury compared with the single gene deficiencies; however, this did not translate to other end points such as plasma creatinine levels or the number of TUNEL-positive cells (Figure 4, B–E). We conclude that crystal-induced tissue injury involves PPIF and MLKL, suggesting that both MPT-RN and necroptosis are involved. In addition, their partially redundant roles in crystalline AKI imply a collaborative interaction of these two signaling pathways *in vivo*.

### MPT-RN and Necroptosis-Targeted Pharmaceutical Interventions Abrogate Crystalline Organ Injury and Failure

To test whether PPIF could be a molecular target for therapeutic intervention and to determine the potential of dual MPT-RN/necroptosis blockade, we treated wild-type mice with the MPT inhibitor cyclosporin A, the necroptosis inhibitor necrostatin-1s, or both. Oxalate exposure induced equal amounts of renal CaOx crystal deposits in mice of all groups (Figure 5A). Cyclosporin A and necrostatin-1s had comparable partial renoprotective effects on plasma creatinine levels as a marker of AKI and on tubular injury and the number of TUNEL-positive cells (Figure 5, B–E). Dual blockade was more potent than either monotherapy, especially in terms of AKI and TUNEL positivity (Figure 5, B–E). Thus, dual inhibition of MPT- and MLKL-driven necroptosis can elicit some additive effects on crystalline organ failure, but also

this experiment supports functional overlap between the two pathways *in vivo*.

### MPT in Human Tubular Cells and Acute Oxalate Nephropathy

To validate our mouse data in humans, we performed identical experiments on crystal cytotoxicity in HK-2 cells and obtained results identical to those generated with murine cells (Supplemental Figure 8). Then, we used CD24/CD133-positive epithelial progenitor cells isolated from healthy human kidneys, known to contribute to the turnover of tubular epithelial cells and their regeneration upon injury.[13,24] For all crystals tested, the results were identical to the murine cells examined before (Figure 6A, Supplemental Figure 9). Next, we searched a database of 92,000 diagnostic kidney biopsies and identified 1262 cases (1.4%) showing CaOx crystals deposits by light microscopy and birefringence under polarized light. A total of 553 of these 1262 specimens (44%, or 0.6% of total) showed CaOx crystals in the context of acute tubular injury. Furthermore, immunostaining of renal tissue from oxalosis-induced AKI revealed diffuse tubular positivity for PPIF and focal positivity for phosphorylated MLKL in injured cells (Figure 6, B–E). Thus, we conclude that crystal-induced cytotoxicities of human and murine kidney cells are similar and that human tubular epithelial cells also express CYPD and activated MLKL in the context of oxalate crystal-induced AKI.

## DISCUSSION

We had previously shown that CaOx crystal cytotoxicity is caspase-independent, and therefore does not involve apoptosis, but rather regulated necrosis.[8] However, as interfering with necroptosis had been only partially protective, we had hypothesized that crystal cytotoxicity might involve additional pathways of regulated necrosis.[9] Indeed, CaOx crystal cytotoxicity involves phagocytosis and subsequent lysosomal leakage upstream of PPIF-dependent mitochondrial dysfunction, followed by ROS production and necrotic cell death, as previously reported for MPT-RN.[9] Consistently, we found PPIF-dependent MPT-RN to contribute to oxalate crystal-induced AKI. However, the lack of robust additive effects with either dual genetic deficiency or inhibition of the both pathways *in vivo* implies a molecular interference and partial redundancy of these two pathways *in vivo* in our oxalate-induced AKI. These data further unravel the molecular pathophysiology of hyperoxaluria-related AKI and identify PPIF as another potential molecular target to limit kidney injury in this context.

Mitochondrial proteins in the outer or inner mitochondrial membranes have been ascribed important roles in the regulation of inflammation and cell death.[9,25,26] MPT-RN is controlled by PPIF, a mitochondrial matrix protein that is thought to promote the opening of MPT pores. This mechanism drives the breakdown of the mitochondrial outer
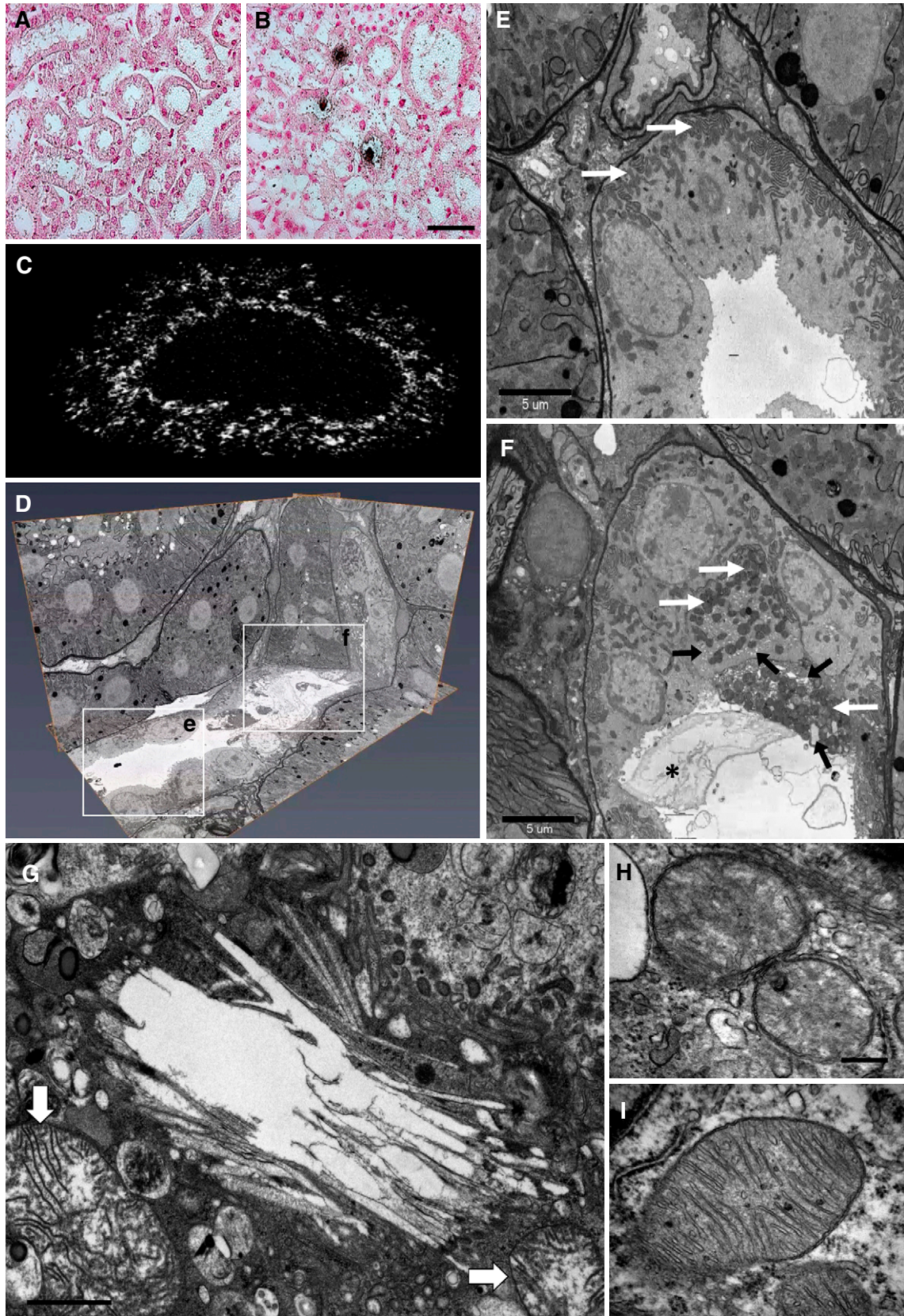
**Figure 3.** Acute oxalate nephropathy involves mitochondrial damage in tubular epithelial cells leading to acute tubular necrosis. (A) Pizzolato staining reveals no crystal deposition in control mice, (B) whereas the presence of diffuse intrarenal crystals in mice
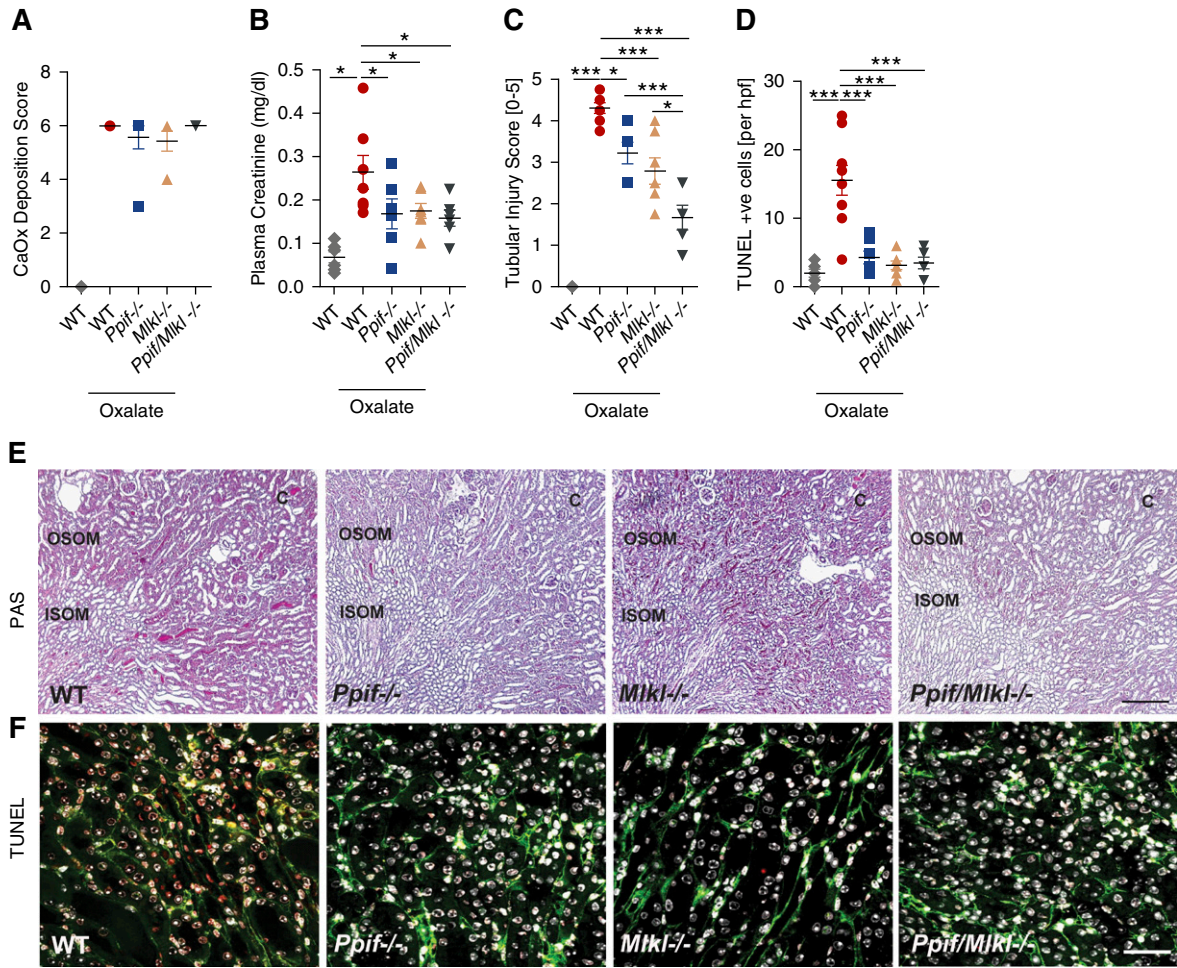
**Figure 4.** Both MPT-induced regulated necrosis and necroptosis contribute to crystalline AKI. (A) Oxalate feeding to wild-type mice as well as to *Ppif-* and *Mlkl-*deficient, and *Ppif/Mlkl* double-deficient mice, of the same genetic background, resulted in identical amounts of CaOx crystal deposition after 24 hours as quantified by morphometry of Pizzolato-stained kidney sections. (B–D) Oxalate nephropathy in wild-type mice was associated with increased (B) plasma creatinine, (C) tubular injury, and (D) TUNEL positive cells, which were attenuated in the gene-deficient mouse strains. PAS staining illustrated tubular necrosis at the corticomedullary junction in wild-type mice. Original image magnification: ×100 (E). TUNEL staining identified dying cells (red), with counterstaining for laminin (green) and cell nuclei (DAPI, white). Original image magnification: ×200 (F). Data are means±SEM from six to nine mice in each group. Data were analyzed using one-way ANOVA with *post hoc* Bonferroni correction and are presented as mean±SEM. *$P<0.05$; ***$P<0.001$ versus oxalate-treated wild-type mice. C, cortex; ISOM, inner stripe of outer medulla; OSOM, outer stripe of outer medulla.

membrane potential, water influx, mitochondrial swelling, loss of cristae, massive ROS production, and ultimately, mitochondrial and cellular demise.[9,25] The biologic significance of this process was documented in several disease contexts by using *Ppif*-deficient mice and small molecule PPIF inhibitors.[12,27,28] In particular, postischemic or radio contrast medium–induced AKI involves PPIF-driven MPT and regulated necrosis,[29,30] although the specific triggers of PPIF activation remained elusive. Our data now demonstrate that CaOx crystal phagocytosis exerts a direct PPIF-driven

exposed to oxalate, (C) which is further confirmed by *ex vivo* kidney computed tomography. Scale bar in (A and B) 50 $\mu$m. (D) SB-EM and 3D reconstruction of a mouse kidney with oxalate nephropathy shows a intact segment of (E) a distal tubule and (F) a segment of the same tubule obstructed segment by a crystal plug. A larger magnification of the left frame (E) shows numerous normal-shaped mitochondria (white arrows) at the basolateral aspect of intact distal tubular epithelial cells. In contrast, a larger magnification of the right frame (F) shows tubule cells exposed to a crystal plug (asterisk) in the tubule lumen as well as numerous intracellular crystals (black arrows) in spatial association to enlarged mitochondria (white arrows) and signs of cell disintegration. Scale bar (E and F) 5 $\mu$m. TEM shows the presence of healthy mitochondria in control mice (H) and damaged mitochondria, as seen by loss of cristae, the presence of lucent matrix, and swollen mitochondria (white arrows) in proximity to intrarenal crystals in mice exposed to oxalate (G and I). Scale bar (G) 1 $\mu$m, (H and I) 250 nm.
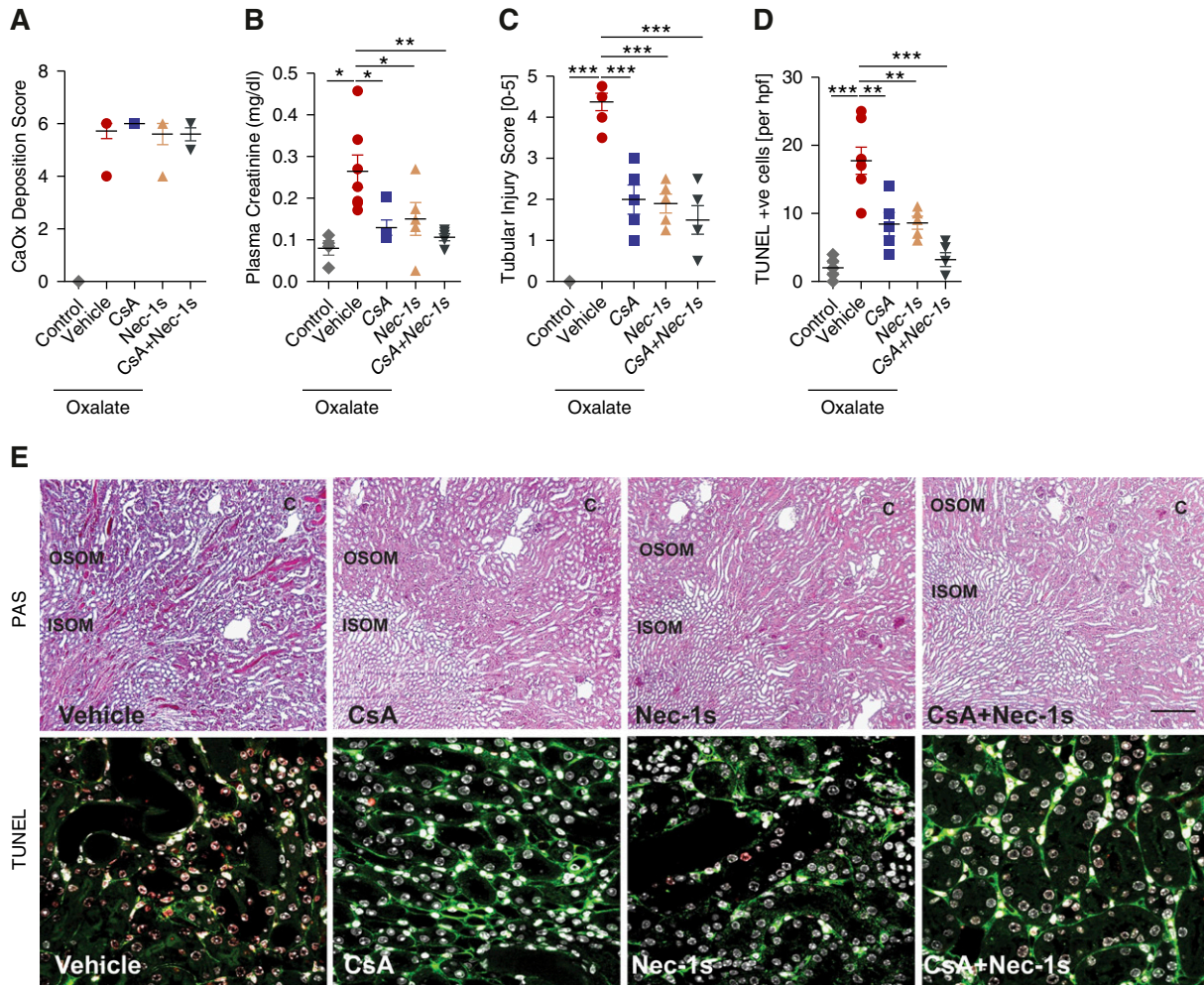
**Figure 5.** Cyclosporin A and necrostatin-1s abrogate crystal nephropathy. (A–D) Oxalate exposure to wild-type mice treated with vehicle, the MPT inhibitor cyclosporine A (CsA; 2 mg/kg), RIP1 kinase inhibitor necrostatin-1s (Nec-1s), or combination of CsA with Nec-1s resulted in (A) identical amounts of CaOx crystal deposition after 24 hours as quantified by morphometry of Pizzolato-stained kidney sections but significantly reduced (B) the levels of plasma creatinine, (C) tubular injury, and (D) the number of TUNEL-positive cells in kidney sections. (E) PAS staining illustrated tubular necrosis at the corticomedullary junction in wild-type mice. Original image magnification: ×100 (E upper panel). TUNEL staining identified dying cells (red), with counterstaining for laminin (green) and cell nuclei (DAPI, white). Original image magnification: ×200 (E lower panel). Data are means±SEM from five to seven mice in each group. Data were analyzed using one-way ANOVA with *post hoc* Bonferroni correction. *$P<0.05$; **$P<0.01$; ***$P<0.001$ versus vehicle-treated mice. C, cortex; ISOM, inner stripe of outer medulla; OSOM, outer stripe of outer medulla.

cytotoxic effect, MPT-related regulated necrosis, on tubular epithelial cells in culture. In mice, this process contributes to oxalate crystal-induced acute tubular necrosis and crystalline AKI independent of CaOx crystallization *per se*, as previously reported.[11,31] In acute oxalate nephropathy, this mechanism adds onto MLKL-driven necroptosis and NLRP3-driven interstitial inflammation, *i.e.*, other molecular pathways directly triggered by crystalline particles within the kidney.[1,7,8] Thus, hyperoxaluria-related AKI presents numerous molecular targets to attenuate organ failure.

The role of mitochondria in CaOx crystal cytotoxicity raises questions on the causative upstream and downstream signals. Our 2D and 3D analysis revealed that even non-professional phagocytes take up CaOx crystals and other microparticles into intracellular endosomal compartments. Indeed, blocking CaOx crystal uptake prevents the loss of the mitochondrial outer membrane potential, ROS production, and necrosis, suggesting CaOx crystal phagocytosis as an upstream event of MPT-related regulated necrosis. Crystalline microparticles are difficult to digest inside phagolysosomes and may cause lysosomal leakage of proteases, a process well described to contribute to crystal-induced activation of the NLRP3 inflammasome.[7,32] In addition, one study indicated that the cysteine cathepsins might cleave RIPK1, an endogenous inhibitor of necroptosis.[33] Indeed, we observed that cathepsin inhibition partially prevented CaOx crystal–induced MPT-related regulated necrosis.
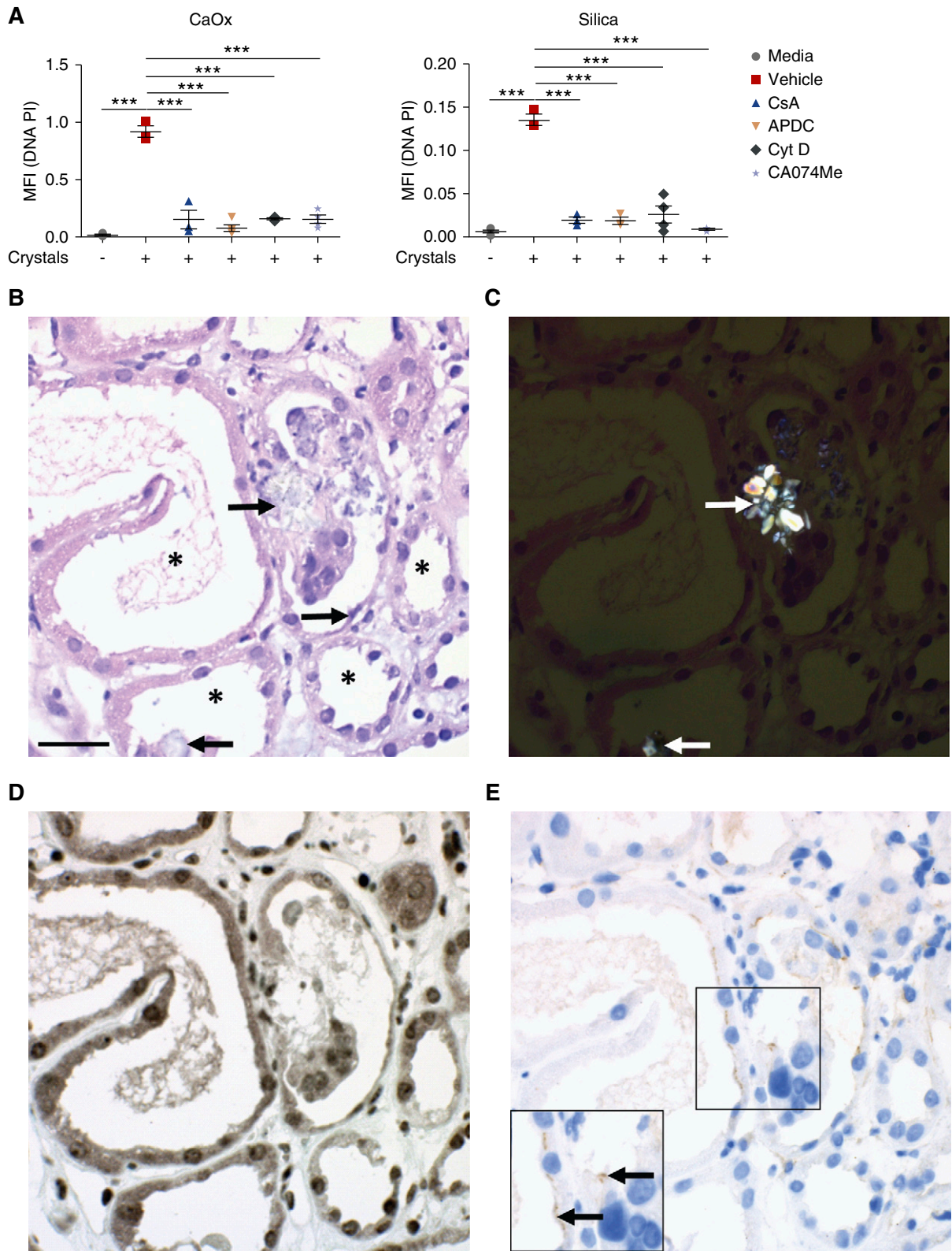
**Figure 6.** Mitochondria permeability transition-related necrosis and necroptosis in human acute oxalate nephropathy. (A) Primary renal human progenitor cells were pretreated with vehicle, CsA (1 $\mu$M), APDC (200 $\mu$M), CytD (10 $\mu$M), and CA074Me (20 $\mu$M) before being exposed to CaOx (1000 $\mu$g/ml) and silica (250 $\mu$g/ml). Cell necrosis was quantified using propidium iodide positivity. Results were expressed as mean fluorescence intensity (MFI) on digital analysis of pictures taken from culture dishes ($n$=3–4). Data are representative from three independent experiments. Data were analyzed using one-way ANOVA and are presented as mean±SEM. ***$P$<0.001
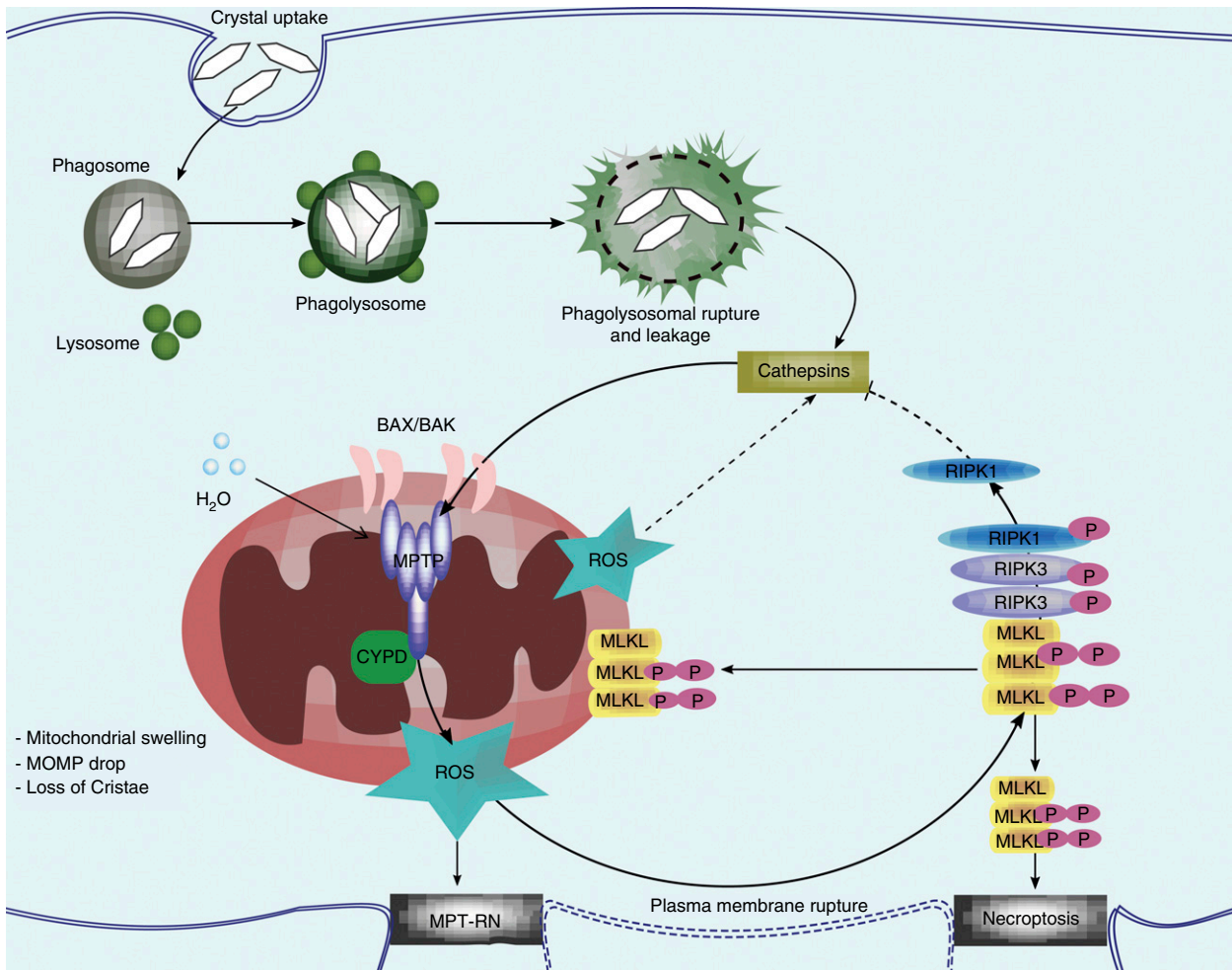
**Figure 7.** Schematic model of the cellular response to CaOx crystal uptake. Bak, Bcl-2 homologous antagonist killer; Bax, Bcl-2-associated X; CYPD, cyclophilin D; MOMP, mitochondrial outer membrane potential; MPTP, mitochondrial permeability transition pore.

The signaling events downstream of MPT are less clear. The release of ROS from mitochondria is considered an essential step in MPT-related regulated necrosis.[9,25] However, it is clear that widespread depletion of mitochondria in cell culture does not affect the kinetics of necroptosis.[34] However, it is appreciated that data have been published on MLKL-driven necroptosis that involves mitochondrial translocation of pMLKL in certain culture conditions.[35–37] As we found that a dual genetic deficiency of *Ppif* or *Mlkl* did not give consistent results across all aspects of AKI, we conclude that at least in hyperoxaluria-induced AKI tested here, MPT-related regulated necrosis and necroptosis are not independent and both involve mitochondrial dysfunction in the context of AKI. Indeed, a recent heart transplant study reported MLKL phosphorylation and necroptosis downstream of PPIF activation.[38] Although dual deficiency of PPIF or MLKL elicited the most potent protective effect on tubular injury, the combinations of two cell death inhibitors with doubtful specificities did not. These data do not exclude independent roles of the both pathways in acute oxalosis, but are consistent with a significant interference of both pathways in crystal cytotoxicity. This finding would be in line with the concept of some redundancy between signaling pathways of regulated necrosis in AKI.[39]

In conclusion, crystal cytotoxicity involves mitochondrial dysfunction and MPT-related regulated necrosis as a form of

versus vehicle. (B–E) Serial sections from human biopsies with oxalate crystal-induced AKI were stained with hematoxylin and eosin and visualized using (B) bright-field microscopy and (C) under polarization. (D) Serial section immunostained for PPIF and (E) immunostaining for p-MLKL. Note the oxalate crystals in consecutive sections marked with white arrows in (C) and with the topmost and the bottom black arrow in (B). Flattened tubular epithelial cells are marked with the black arrow in the middle in (B). Tubular lumina are marked with asterisks in (B). Also, note the diffuse staining of tubular epithelial cells for PPIF (brown) in (D) and the punctate cytoplasmic staining for p-MLKL (brown) in the insert in (E). Original magnification: ×400 for all images, scale bar in (A) represents 20 $\mu$m.

regulated cell death in cell culture and mouse models (Figure 7). Consequently, targeting this pathway, for example, with cyclosporine A, which may have anti-inflammatory capacities beyond inhibition of MPT, may prevent crystal-induced tissue necrosis and organ dysfunction. As interconnections to MLKL-driven necroptosis appear functionally likely, combinations of necrosis inhibitors may exhibit some additive effects, but this needs to be further explored in other crystallopathies.

## ACKNOWLEDGMENTS

## DISCLOSURES

## FUNDING

## SUPPLEMENTAL MATERIAL

This article contains the following supplemental material online at http://jasn.asnjournals.org/lookup/suppl/doi:10.1681/ASN.2018121218/-/DCSupplemental.

Supplemental Figure 1.
Supplemental Figure 2.
Supplemental Figure 3.
Supplemental Figure 4.
Supplemental Figure 5.
Supplemental Figure 6.
Supplemental Figure 7.
Supplemental Figure 8.
Supplemental Figure 9.
Supplemental Video 1.
Supplemental Video 2.
Supplemental Video 3.
Supplemental Appendix 1. Supplemental methods and references.

## REFERENCES

1. Mulay SR, Anders HJ: Crystal nephropathies: Mechanisms of crystal-induced kidney injury. *Nat Rev Nephrol* 13: 226–240, 2017
2. Mulay SR, Anders HJ: Crystallopathies. *N Engl J Med* 374: 2465–2476, 2016
3. Syed F, Mena-Gutierrez A, Ghaffar U: A case of iced-tea nephropathy. *N Engl J Med* 372: 1377–1378, 2015
4. Nankivell BJ, Murali KM: Images in clinical medicine. Renal failure from vitamin C after transplantation. *N Engl J Med* 358: e4, 2008
5. Morfin J, Chin A: Images in clinical medicine. Urinary calcium oxalate crystals in ethylene glycol intoxication. *N Engl J Med* 353: e21, 2005
6. Karaolanis G, Lionaki S, Moris D, Palla VV, Vernadakis S: Secondary hyperoxaluria: A risk factor for kidney stone formation and renal failure in native kidneys and renal grafts. *Transplant Rev (Orlando)* 28: 182–187, 2014
7. Mulay SR, Kulkarni OP, Rupanagudi KV, Migliorini A, Darisipudi MN, Vilaysane A, et al.: Calcium oxalate crystals induce renal inflammation by NLRP3-mediated IL-1β secretion. *J Clin Invest* 123: 236–246, 2013
8. Mulay SR, Desai J, Kumar SV, Eberhard JN, Thomasova D, Romoli S, et al.: Cytotoxicity of crystals involves RIPK3-MLKL-mediated necroptosis. *Nat Commun* 7: 10274, 2016
9. Galluzzi L, Vitale I, Aaronson SA, Abrams JM, Adam D, Agostinis P, et al.: Molecular mechanisms of cell death: Recommendations of the Nomenclature Committee on cell death 2018. *Cell Death Differ* 25: 486–541, 2018
10. Nakagawa T, Shimizu S, Watanabe T, Yamaguchi O, Otsu K, Yamagata H, et al.: Cyclophilin D-dependent mitochondrial permeability transition regulates some necrotic but not apoptotic cell death. *Nature* 434: 652–658, 2005
11. Niimi K, Yasui T, Okada A, Hirose Y, Kubota Y, Umemoto Y, et al.: Novel effect of the inhibitor of mitochondrial cyclophilin D activation, N-methyl-4-isoleucine cyclosporin, on renal calcium crystallization. *Int J Urol* 21: 707–713, 2014
12. Baines CP, Kaiser RA, Purcell NH, Blair NS, Osinska H, Hambleton MA, et al.: Loss of cyclophilin D reveals a critical role for mitochondrial permeability transition in cell death. *Nature* 434: 658–662, 2005
13. Angelotti ML, Ronconi E, Ballerini L, Peired A, Mazzinghi B, Sagrinati C, et al.: Characterization of renal progenitors committed toward tubular lineage and their regenerative potential in renal tubular injury. *Stem Cells* 30: 1714–1725, 2012
14. Deerinck TJ, Bushong EA, Thor A, Ellisman MH: NCMIR Methods for 3D EM: A new protocol for preparation of biological specimens for serial block face scanning electron microscopy. *Microscopy*, 6–8, 2010
15. Belevich I, Joensuu M, Kumar D, Vihinen H, Jokitalo E: Microscopy image browser: A platform for segmentation and analysis of multidimensional datasets. *PLoS Biol* 14: e1002340, 2016
16. Dabov K, Foi A, Katkovnik V, Egiazarian K: Image denoising by sparse 3-D transform-domain collaborative filtering. *IEEE Trans Image Process* 16: 2080–2095, 2007

17. Meyer F: Topographic distance and watershed lines. *Signal Processing* 38: 113–125, 1994

18. Achanta R, Shaji A, Smith K, Lucchi A, Fua P, Süsstrunk S: SLIC super-pixels compared to state-of-the-art superpixel methods. *IEEE Trans Pattern Anal Mach Intell* 34: 2274–2282, 2012

19. Boykov Y, Kolmogorov V: An experimental comparison of min-cut/max-flow algorithms for energy minimization in vision. *IEEE Trans Pattern Anal Mach Intell* 26: 1124–1137, 2004

20. Murphy JM, Czabotar PE, Hildebrand JM, Lucet IS, Zhang JG, Alvarez-Diaz S, et al.: The pseudokinase MLKL mediates necroptosis via a molecular switch mechanism. *Immunity* 39: 443–453, 2013

21. Martinon F, Pétrilli V, Mayor A, Tardivel A, Tschopp J: Gout-associated uric acid crystals activate the NALP3 inflammasome. *Nature* 440: 237–241, 2006

22. Hornung V, Bauernfeind F, Halle A, Samstad EO, Kono H, Rock KL, et al.: Silica crystals and aluminum salts activate the NALP3 inflammasome through phagosomal destabilization. *Nat Immunol* 9: 847–856, 2008

23. Khan SR: Nephrocalcinosis in animal models with and without stones. *Urol Res* 38: 429–438, 2010

24. Lazzeri E, Angelotti ML, Peired A, Conte C, Marschner JA, Maggi L, et al.: Endocycle-related tubular cell hypertrophy and progenitor pro-liferation recover renal function after acute kidney injury. *Nat Commun* 9: 1344, 2018

25. Vanden Berghe T, Linkermann A, Jouan-Lanhouet S, Walczak H, Vandenabeele P: Regulated necrosis: The expanding network of non-apoptotic cell death pathways. *Nat Rev Mol Cell Biol* 15: 135–147, 2014

26. Mao F, Tu Q, Wang L, Chu F, Li X, Li HS, et al.: Mesenchymal stem cells and their therapeutic applications in inflammatory bowel disease. *Oncotarget* 8: 38008–38021, 2017

27. Schinzel AC, Takeuchi O, Huang Z, Fisher JK, Zhou Z, Rubens J, et al.: Cyclophilin D is a component of mitochondrial permeability transition and mediates neuronal cell death after focal cerebral ischemia. *Proc Natl Acad Sci U S A* 102: 12005–12010, 2005

28. Shore ER, Awais M, Kershaw NM, Gibson RR, Pandalaneni S, Latawiec D, et al.: Small molecule inhibitors of Cyclophilin D to protect mitochondrial function as a potential treatment for acute pancreatitis. *J Med Chem* 59: 2596–2611, 2016

29. Linkermann A, Bräsen JH, Darding M, Jin MK, Sanz AB, Heller JO, et al.: Two independent pathways of regulated necrosis mediate ischemia-reperfusion injury. *Proc Natl Acad Sci U S A* 110: 12024–12029, 2013

30. Park JS, Pasupulati R, Feldkamp T, Roeser NF, Weinberg JM: Cyclophilin D and the mitochondrial permeability transition in kidney proximal tubules after hypoxic and ischemic injury. *Am J Physiol Renal Physiol* 301: F134–F150, 2011

31. Niimi K, Yasui T, Hirose M, Hamamoto S, Itoh Y, Okada A, et al.: Mitochondrial permeability transition pore opening induces the initial process of renal calcium crystallization. *Free Radic Biol Med* 52: 1207–1217, 2012

32. Franklin BS, Mangan MS, Latz E: Crystal formation in inflammation. *Annu Rev Immunol* 34: 173–202, 2016

33. McComb S, Shutinoski B, Thurston S, Cessford E, Kumar K, Sad S: Cathepsins limit macrophage necroptosis through cleavage of Rip1 kinase. *J Immunol* 192: 5671–5678, 2014

34. Tait SW, Oberst A, Quarato G, Milasta S, Haller M, Wang R, et al.: Widespread mitochondrial depletion via mitophagy does not com-promise necroptosis. *Cell Reports* 5: 878–885, 2013

35. Karch J, Kanisicak O, Brody MJ, Sargent MA, Michael DM, Molkentin JD: Necroptosis interfaces with MOMP and the MPTP in mediating cell death. *PLoS One* 10: e0130520, 2015

36. Sun W, Wu X, Gao H, Yu J, Zhao W, Lu JJ, et al.: Cytosolic calcium mediates RIP1/RIP3 complex-dependent necroptosis through JNK activation and mitochondrial ROS production in human colon cancer cells. *Free Radic Biol Med* 108: 433–444, 2017

37. Sureshbabu A, Patino E, Ma KC, Laursen K, Finkelsztein EJ, Akchurin O, et al.: RIPK3 promotes sepsis-induced acute kidney injury via mito-chondrial dysfunction. *JCI Insight* 3(11) 98411, 2018

38. Gan I, Jiang J, Lian D, Huang X, Fuhrmann B, Liu W, et al.: Mitochondrial permeability regulates cardiac endothelial cell necroptosis and cardiac allograft rejection. *Am J Transplant* 19: 686–698, 2018

39. Linkermann A: Nonapoptotic cell death in acute kidney injury and transplantation. *Kidney Int* 89: 46–57, 2016

## AFFILIATIONS

[1]Division of Nephrology, Department of Medicine IV, University Hospital, LMU Munich, Munich, Germany; [2]Pharmacology Division, CSIR-Central Drug Research Institute, Lucknow, India; [3]Biomedical Center, Core Facility Animal Models, Ludwig Maximilian University, Planegg-Martinsried, Germany; [4]Division of Nephrology, Institute of Pathology, Rheinisch-Westfälische Technische Hochschule University of Aachen, Aachen, Germany; [5]Division of Nephrology, Department of Internal Medicine III, University Hospital Carl Gustav Carus at the Technische Universität Dresden, Dresden, Germany; [6]Department of Pathology and Immunology, School of Medicine, Washington University in St. Louis, St. Louis, Missouri; [7]Arkana Laboratories, Little Rock, Arkansas; [8]Department of Histology, Cytology, and Embryology, Danylo Halytsky Lviv National Medical University, Lviv, Ukraine; [9]Department of Internal Medicine 3, University of Erlangen-Nuremberg, Erlangen, Germany; [10]Excellence Centre for Research, Transfer and High Education for the Development of De Novo Therapies, University of Florence, Florence, Italy; [11]Electron Microscopy Unit, Institute of Biotechnology, University of Helsinki, Helsinki, Finland; and [12]Institute of Pathology, University of Cologne, Cologne, Germany